Safe Lane-Keeping With Feedback Delay: Bifurcation Analysis and Experiments

Illés Vörös, Dénes Takács, and Gábor Orosz, *Senior Member, IEEE*

***Abstract*—A lane-keeping controller for automobiles is analyzed in this letter, with the consideration of time delay in the feedback loop. Unstable periodic orbits are identified inside the linearly stable domain of control gains. Based on the amplitude of these unstable solutions, safe parameter zones are identified, where the closed loop system is robust against perturbations, i.e., where the basin of attraction of the stable equilibrium is sufficiently large. Sensitivity to perturbations in different regions of linearly stable control gains is demonstrated by a series of real-vehicle experiments. Finally, modifications of the control law are proposed that lead to significant improvements in terms of the robustness against perturbation for the controlled vehicle, achieving global stability in the practical sense.**

***Index Terms*—Automated vehicles, path-following control, bifurcations, limit cycles, time delay.**

I. Introduction

ADVANCED driver assistance systems such as lane-keeping and lane-changing controllers have the potential to significantly reduce the number of road accidents caused by unintended lane departures [1]. In order to guarantee stable and safe operation of these driving functions under all potential circumstances, the corresponding steering controllers need to be designed with a high degree of robustness against perturbations.

One of the main bottlenecks of these controllers is the presence of feedback delay in the control loop, which includes effects such as sensor delay (arising from GPS as well as from optical sensors), computation time of the estimation and control algorithms, as well as delays arising from actuation. It has been shown that these delay effects lead to a significant decrease in the domain of stabilizing control gains, reduce control performance and can even lead to instability [2], [3], [4].

On the other hand, nonlinear phenomena, such as sensitivity to perturbations in the presence of limit cycles (periodic orbits) are often not considered in the traditional methods of linear control design [3]. In the literature, the nonlinear dynamics of automobiles have mostly been analyzed with a focus on the cornering behavior of the vehicle without control action [5], [6], [7], or with the consideration of a human driver [8], [9], [10]. Understanding the nonlinear dynamics of the controlled vehicle is also essential to design high-performance controllers that are able to drive the vehicle at its handling limits [11], [12], [13], [14].

This letter presents the nonlinear analysis of a lane-keeping controller with feedback delay, with an emphasis on ensuring that the vehicle can safely handle unexpected disturbances (e.g., hitting an ice patch) and highly dynamic maneuvers, such as emergency obstacle avoidance. This is achieved by uncovering unstable limit cycles around the linearly stable equilibrium corresponding to the rectilinear motion. The amplitudes of the unstable limit cycles are used to quantify a sensitivity of the system to perturbations, i.e., whether perturbations cause the vehicle to produce undesired oscillations even if the control gains are selected from the linearly stable domain. Based on our analysis, a so-called safe zone of control gains is identified inside the linearly stable domain in the parameter space, where the vehicle is robust against perturbations of given size, which can be used as a guideline when tuning the controller.

The sensitivity of the controlled vehicle to perturbations is also demonstrated in a series of real-vehicle measurements performed on the Mcity test track of the University of Michigan. The measurement results confirm the presence and the approximate location of the safe zone of control gains. Finally, we show that by shaping the input signal with an appropriate wrapper function, the amplitude of the unstable limit cycles can be greatly extended, leading to a significant expansion of the basin of attraction of the equilibrium and achieving global stability in the practical sense.

The rest of the letter is organized as follows: the model of the controlled vehicle is presented in Section II. The nonlinear analysis of the system is performed in Section III using numerical continuation and the corresponding experimental results are detailed in Section IV. In Section V, the nonlinear

Manuscript received 16 September 2022; revised 21 November 2022; accepted 9 December 2022. Date of publication 23 December 2022; date of current version 6 January 2023. This work was supported in part by the János Bolyai Research Scholarship of the Hungarian Academy of Sciences; in part by the National Research, Development and Innovation Office of Hungary under Grant NKFI-128422 and Grant 2020-1.2.4-TÉT-IPARI-2021-00012; and in part by Mcity at University of Michigan. Recommended by Senior Editor L. Zhang. *(Corresponding author: Illés Vörös.)*

Illés Vörös is with the Department of Applied Mechanics, Budapest University of Technology and Economics, 1111 Budapest, Hungary (e-mail: illes.voros@mm.bme.hu).

Dénes Takács is with the ELKH-BME Research Group on Dynamics of Machines, 1111 Budapest, Hungary (e-mail: takacs@mm.bme.hu).

Gábor Orosz is with the Department of Mechanical Engineering and the Department of Civil and Environmental Engineering, University of Michigan, Ann Arbor, MI 48109 USA (e-mail: orosz@umich.edu).

Digital Object Identifier 10.1109/LCSYS.2022.3231823

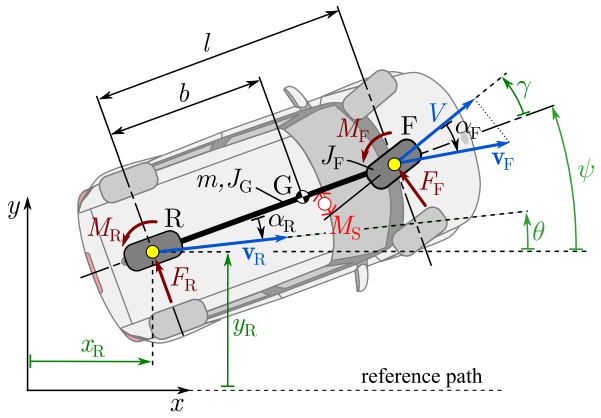

Fig. 1. Bicycle model with steering dynamics.

control law with the wrapper function is presented, and the improvements in the nonlinear performance of the vehicle are demonstrated. The results are concluded in Section VI.

II. Vehicle Model and Control Design

The vehicle model considered in this letter is the in-plane bicycle model extended with steering dynamics, as shown in Fig. 1. The center points of the front and rear axles are denoted by F and R, respectively, while G marks the center of mass. The generalized coordinates that describe the vehicle configuration consist of the position x_R and y_R of point R, the yaw angle ψ, and the steering angle γ. Assuming a front-wheel drive vehicle, the wheel directional velocity component of the front wheel is kept at a constant value V.

The geometrical parameters include the wheelbase l and the distance b between points R and G. The vehicle mass is denoted by m, while J_G is the yaw moment of inertia about the center of mass and J_F denotes the mass moment of inertia of the steering system. Deriving the equations of motion of the vehicle model using the Appell-Gibbs method (see [15] for details) leads to

$$\dot{x}_R = V\frac{\cos\psi}{\cos\gamma} - \sigma\frac{\sin(\psi+\gamma)}{\cos\gamma} - l\omega\cos\psi\tan\gamma, \tag{1}$$

$$\dot{y}_R = V\frac{\cos\psi}{\cos\gamma} + \sigma\frac{\cos(\psi+\gamma)}{\cos\gamma} - l\omega\sin\psi\tan\gamma, \tag{2}$$

$$\dot{\psi} = \omega, \tag{3}$$

$$\dot{\gamma} = \Omega, \tag{4}$$

$$\begin{bmatrix} m_{11} & m_{12} & 0 \\ m_{21} & m_{22} & J_F \\ 0 & J_F & J_F \end{bmatrix}\begin{bmatrix} \dot{\sigma} \\ \dot{\omega} \\ \dot{\Omega} \end{bmatrix} = \begin{bmatrix} f_1 \\ f_2 \\ f_3 \end{bmatrix}, \tag{5}$$

where σ is the lateral velocity of point R, ω is the yaw rate of the vehicle, and Ω is the steering rate. The generalized mass matrix includes the elements

$$m_{11} = \frac{m}{\cos^2\gamma}, \tag{6}$$

$$m_{12} = m_{21} = m\left(b + l\tan^2\gamma\right), \tag{7}$$

$$m_{22} = J_G + J_F + m\left(b^2 + l^2\tan^2\gamma\right), \tag{8}$$

while the right-hand side of (5) consists of

$$f_1 = \frac{F_F}{\cos\gamma} + F_R - \frac{m}{\cos\gamma}(V-(l-b)\omega\sin\gamma)\omega + \frac{m\sin\gamma}{\cos^3\gamma}(V\sin\gamma - \sigma - l\omega)\Omega, \tag{9}$$

$$f_2 = \frac{F_F l}{\cos\gamma} - \frac{m}{\cos\gamma}(bV + (l-b)\sigma\sin\gamma)\omega + \frac{ml\sin\gamma}{\cos^3\gamma}(V\sin\gamma - \sigma - l\omega)\Omega + M_F + M_R, \tag{10}$$

$$f_3 = M_F + M_S. \tag{11}$$

The lateral tire forces F_F and F_R, as well as the self-aligning moments M_F and M_R are considered as functions of the side-slip angles

$$\tan\alpha_F = -\frac{\sigma + l\omega}{V\cos\gamma} + \tan\gamma, \tag{12}$$

$$\tan\alpha_R = \frac{V\cos\gamma}{-V + (\sigma + l\omega)\sin\gamma}, \tag{13}$$

and we use the nonlinear brush tire model detailed in [15]. The front wheels are steered by the steering torque M_S, which is generated by the steering motor.

In order to ensure stable path following, a higher-level controller is designed in this letter to follow the straight-line reference path along the x–axis. The desired steering angle γ^{des} is calculated using the feedback of the lateral position y_R and the course angle θ of the rear axle center point R:

$$\gamma^{des}(t) = -k_y y_R(t-\tau) - k_\theta\theta(t-\tau). \tag{14}$$

Here τ is the overall feedback delay, incorporating the delays in sensing, data processing and actuation. The course angle (heading angle of point R) is calculated as $\theta = \psi - \alpha_R$, and k_y and k_θ are the control gains. In case of varying path curvature, the tracking performance of this simple controller can be improved by adding a feedforward term, as shown in [16]. To realize the desired steering angle, the steering torque M_S is generated according to the lower-level PID controller

$$M_S = -k_p\left(\gamma - \gamma^{des}\right) - k_d\dot{\gamma} - k_i z, \tag{15}$$

where k_p, k_d and k_i are the lower-level control gains and

$$\dot{z} = \gamma - \gamma^{des}. \tag{16}$$

The nonlinear system (1)-(16) describes the dynamics of the controlled vehicle. In the next section we analyze the linear and nonlinear dynamics of this system and compute the unstable limit cycles which determine the region of attraction of the equilibrium (rectilinear motion).

III. Nonlinear Analysis

The linear stability of the controlled vehicle can be ensured by analyzing the characteristic equation of the closed-loop system linearized around the equilibrium i.e., the rectilinear motion. Considering that the vehicle is moving along the x–axis, the equilibrium is given by $x_R = Vt$, $y_R \equiv 0$, $\psi \equiv 0$, $\gamma \equiv 0$, $\sigma \equiv 0$, $\omega \equiv 0$, $\Omega \equiv 0$, $z \equiv 0$. Here we briefly describe the linear stability analysis while more details can be found

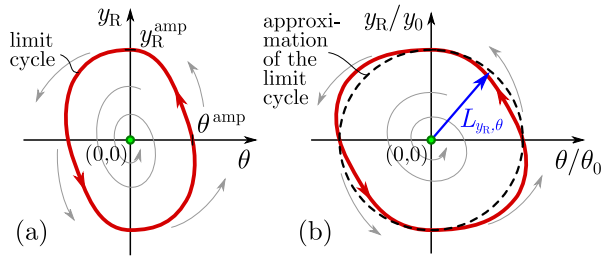

Fig. 2. (a) Phase portrait with a stable equilibrium (green) and an unstable limit cycle (red) in the (y_R, θ) plane. (b) Introduction of the $L_{y_R,\theta}$ norm.

in [15] and [3]. Because of the time delay τ in the control law in (14), the characteristic equation contains $e^{-s\tau}$ beside the polynomials of poles s. For such transcendental equations, among other methods, the D-subdivision [17] can be used to determine the linear stability boundaries. Fig. 3(c) depicts the stability boundary (black curve) in the plane of the two higher-level control gains k_θ and k_y. The rectilinear motion is linearly stable in the union of the gray shaded and colored domains and unstable otherwise.

However, the linear stability of the system only provides information about the local dynamics near the equilibrium. In order to unveil what kinds of dynamics can happen farther from the equilibrium, the methods of nonlinear analysis are used in the remainder of this section. In particular, we want to ensure that when the equilibrium is stable in the linear sense, its basin of attraction is large enough in order to enable the vehicle to safely handle larger perturbations, such as the appearance of an unexpected obstacle.

We found that the linear stability loss corresponds to subcritical Hopf bifurcations in the nonlinear system [18]. This means that even when the equilibrium is linearly stable, it is surrounded by an unstable limit cycle (periodic orbit); see the phase portrait in the (y_R, θ) plane in Fig. 2(a). The basin of attraction of the stable equilibrium is bounded by this unstable limit cycle (in the infinite dimensional state space). Thus, large enough perturbations may push the system outside the limit cycle and make it diverge from the locally stable equilibrium. That is, the size of the limit cycle corresponds to the sensitivity of the controlled system against perturbations. To quantify this sensitivity, one can characterize the size of the limit cycle using different norms. A meaningful choice is to use the amplitude y_R^{amp} of the limit cycle. While this has a clear physical interpretation, it does not capture the sensitivity against the perturbations in other states. Hence, we introduce the dimensionless custom norm

$$L_{y_R,\theta} = \sqrt{\left(\frac{y_R}{y_0}\right)^2 + \left(\frac{\theta}{\theta_0}\right)^2}. \tag{17}$$

We choose $y_0 = 1\,\text{m}$ and $\theta_0 = 0.08\,\text{rad}$ (determined based on the average value of θ^{amp}/y_R^{amp} within the domain of stable control gains). Using this norm, we can approximate the limit cycle as a circle in the dimensionless phase portrait, see Fig. 2(b), and characterize the sensitivity of the system against the perturbations in the combination of the lateral position y_R and the course angle θ.

To investigate how the basin of attraction changes while varying the control gains we compute the limit cycle using numerical collocation and follow the branch of the limit cycle using numerical continuation, namely, the software, DDE-Biftool [19]. The bifurcation diagrams in Fig. 3(a) and (b) depict the amplitude of the limit cycle in the lateral position y_R and in the $L_{y_R,\theta}$ norm as the control gain k_θ is varied, for the vehicle parameters listed in Table I. Observe that the branch of the unstable limit cycle emerges from the Hopf bifurcation points which mark the linear stability boundary of the equilibrium. The amplitude of the limit cycle, and correspondingly the size of the basin of attraction of the equilibrium, changes with the parameter k_θ.

TABLE I
VEHICLE PARAMETERS

Parameter	Value
Vehicle wheelbase (l)	2.57 m
Distance between rear axle and center of gravity (b)	1.54 m
Vehicle mass (m)	1770 kg
Yaw moment of inertia (J_G)	1343 kgm^2
Steering system moment of inertia (J_F)	0.25 kgm^2
Lower-level steering control proportional gain (k_p)	640 Nm
Lower-level derivative gain (k_d)	8 Nms
Lower-level integral gain (k_i)	40 Nm/s
Longitudinal velocity (V)	15 m/s
Total time delay in control loop (τ)	0.7 s

The results of the nonlinear analysis are summarized in Fig. 3(c), where the colormap indicates the sensitivity of the controlled vehicle to perturbations across the domain of linearly stable control gain combinations. A region of safe zone of control gains is also identified (indicated by gray shading), where the limit cycle amplitudes in terms of y_R do not fall below 2 meters, indicating that the vehicle can safely handle larger perturbations. Observe that a large part of the linearly stable parameter domain falls outside of this safe zone. In these cases the system can leave the basin of attraction of the stable equilibrium for sufficiently large perturbations, which is a severe safety issue in practice.

IV. EXPERIMENTAL VALIDATION

To validate the results of the bifurcation analysis, a series of real-vehicle experiments were performed at the Mcity test track of the University of Michigan. The test vehicle (shown in Fig. 3(d) and detailed in [15]) was equipped with a GPS device mounted at the rear axle center point R. The experiments were aimed at demonstrating the feasibility of motion control relying on vehicle-to-everything (V2X) communication only, in cases when the onboard sensors fail [15]. This means that the applied control algorithms must handle less frequent data transfer and less accurate sensor data. In case of the GPS device used in the experiments, the satellite data was upgraded only every 1 sec (with state estimations in-between) with an accuracy of ≈0.7 m.

Experiments were performed for different combinations of the higher-level control gains, where the vehicle aimed to follow the lane centerline of a straight segment of the test track, relying on GPS data. For each control gain combination in Fig. 3(e), test runs were carried out with different initial lateral positions and orientations of the vehicle. Depending on the behavior of the vehicle, the individual measurement

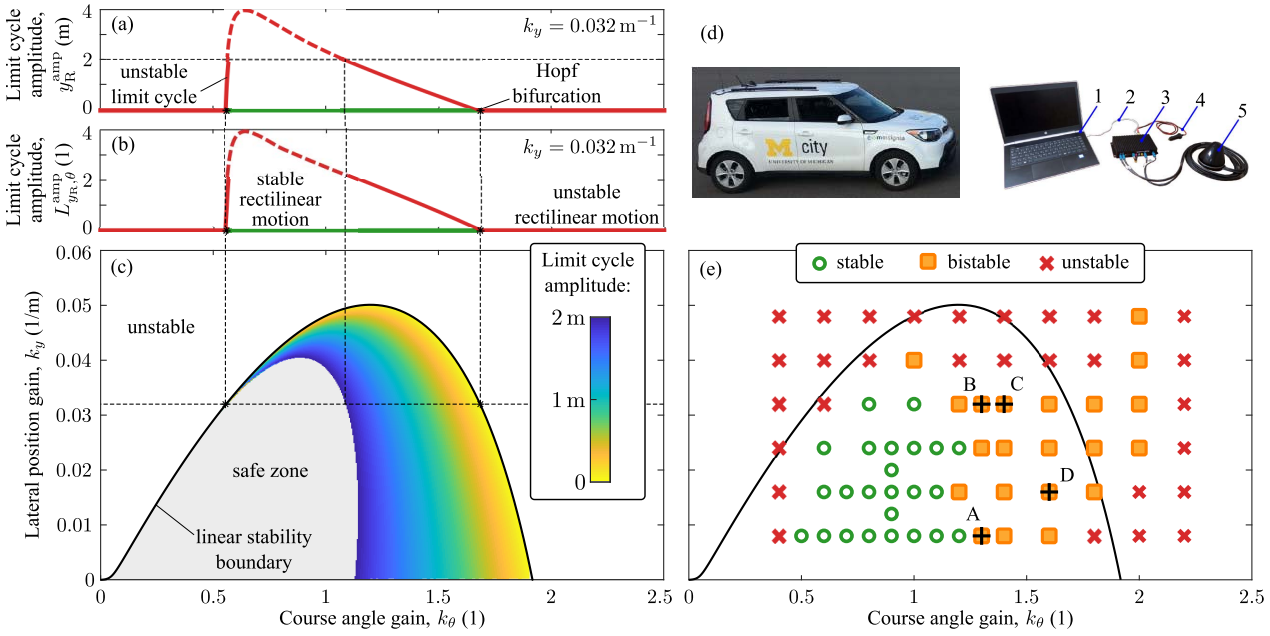

Fig. 3. (a)-(b) Bifurcation diagrams of the controlled vehicle. (c) Stability chart where the coloring refers to the unstable limit cycle amplitudes. (d) Vehicle and V2X measurement setup used in the experiments – 1: host computer, 2: network cable, 3: electronic control unit, 4: power cable, 5: antennae. (e) Experimental results.

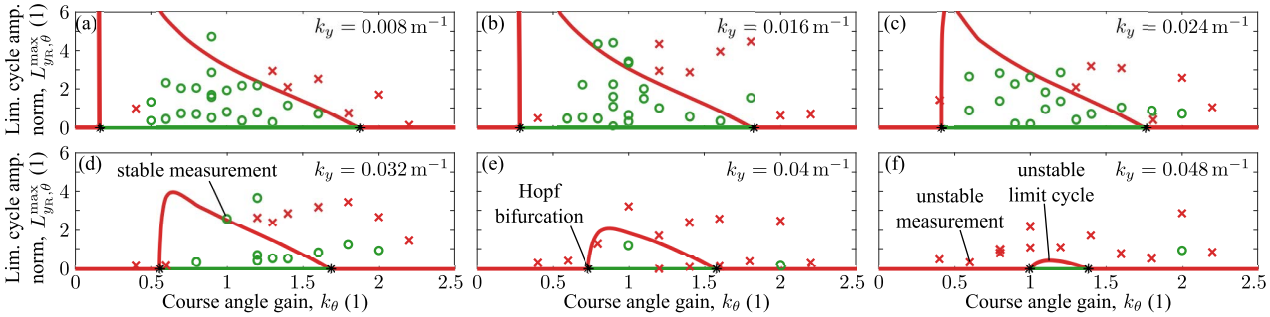

Fig. 4. Bifurcation diagrams comparing the theoretical and the experimental results. The vertical axis corresponds to the norm defined in (17).

points were labelled as either stable (green circles), bistable (orange squares) or unstable (red crosses). For the gain combinations labelled as stable, the lane-keeping controller was working as intended in all test runs, with decaying oscillations. In the measurement points labelled as bistable, solutions with increasing and decreasing lateral oscillations were both observed. Finally, in the points labelled as unstable, the vehicle was not able to successfully follow the lane centerline in any of the test runs. Comparing the results in panels (c) and (e) of Fig. 3 shows that consistently stable measurements regardless of initial perturbations were achieved using control gains that are approximately located in the theoretically determined safe zone.

Figure 4 shows bifurcation diagrams comparing the theoretical and the experimental results while varying the two control gains. Good correspondence can be found between the theoretical and the experimental results: apart from a few outliers, it can be clearly seen that smaller control gains can handle larger perturbations better, and there is both a lower and an upper limit of the stable domain in terms of k_θ.

The measured vehicle trajectories are plotted in Fig. 5 using the control gains in points A, B, C and D in Fig. 3(e). The panels in the left column show the trajectories in the plane of the lateral position and the course angle, along with the corresponding unstable limit cycles computed based on the model. The panels on the right show the vehicle position along the test track. It can be seen that depending on the initial conditions, the same control gains can lead to stable path following or instability. It has to be kept in mind though, that the actual state space of the system includes the rest of the state variables, as well as the infinite dimensional initial functions too. Therefore the limit cycles in these sections of the state space do not exactly correspond to the boundaries of the basin of attraction of the stable equilibrium.

V. Extension of the Safe Zone

The theoretical and experimental investigations above highlight that nonlinearity in the dynamics leads to unwanted performance when using controllers designed based on the linearized dynamics. To improve the nonlinear behavior of

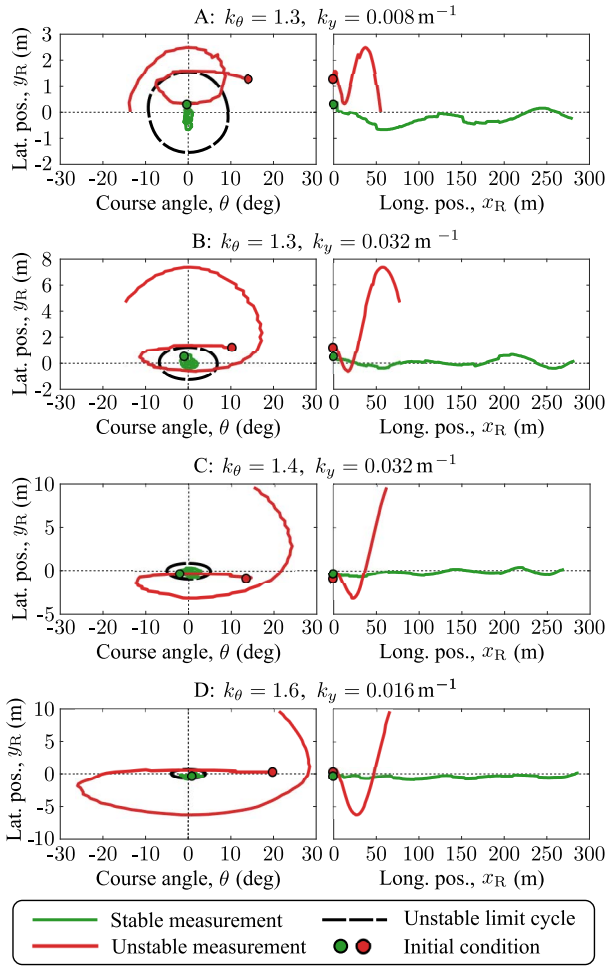

Fig. 5. Stable and unstable measured vehicle trajectories and the corresponding theoretical unstable limit cycles.

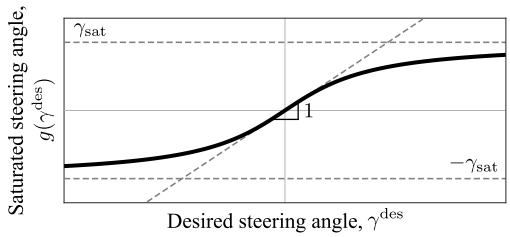

Fig. 6. The continuous wrapper function $g(\gamma^{\mathrm{des}})$ in (18).

the controlled vehicle, additional nonlinearity can be introduced in the control law, which, once appropriately chosen, may compensate the negative effects of the nonlinearity in the dynamics. Here we propose a nonlinear extension of the control law (14) and demonstrate that this can increase the safe zone of stabilizing control gains and result in global stability in the practical sense.

In particular, the control law (14) is wrapped with the continuous wrapper function:

$$g(\gamma^{\mathrm{des}}) = \frac{2\gamma_{\mathrm{sat}}}{\pi} \arctan\left(\frac{\pi}{2\gamma_{\mathrm{sat}}}\gamma^{\mathrm{des}}\right), \tag{18}$$

see [16]. As shown in Fig. 6, the wrapper function has the gradient 1 at $\gamma^{\mathrm{des}} = 0$, that is, it does not influence the linear stability of the equilibrium. Also, it saturates at $\pm\gamma_{\mathrm{sat}}$ as $\gamma^{\mathrm{des}} \to \infty$. Notice, however, that smaller steering angles are also affected. This wrapper function allows the use of larger control gains, which leads to better tracking performance at small errors, while the gains are gradually reduced for large errors in order to "soften" the response of the controller.

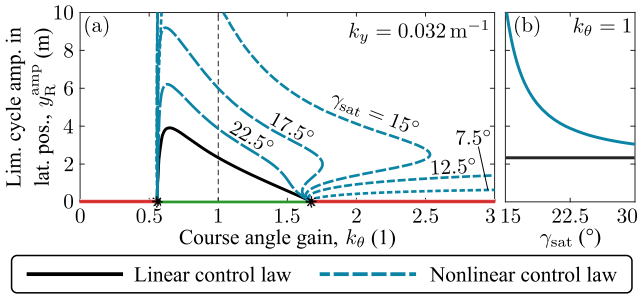

Fig. 7. (a) Bifurcation diagram using the linear (black) and the nonlinear (blue) control law with different saturation levels γ_{sat}. (b) Limit cycle amplitude as a function of the saturation parameter γ_{sat}.

We present the results of the bifurcation analysis of system (1)-(16) with the wrapper function (18) for different values of the saturation limit γ_{sat} in Fig. 7(a). One may observe that decreasing γ_{sat} leads to a sharp increase in the limit cycle amplitudes and consequently the expansion of the basin of attraction of the stable equilibrium. This is quantified in Fig. 7(b) by plotting the amplitude of the limit cycle as a function of γ_{sat} for the gain combination $k_y = 0.032\,\mathrm{m}^{-1}$, $k_\theta = 1$. As the same trend is observed for other gain combinations, the safe zone expands in the parameter space. For small enough value γ_{sat} the branch of the limit cycle breaks and there exist no unstable limit cycle within the majority of the linearly stable domain. As a result, the safe zone covers almost the entire stable domain. This means that the previously shown strong sensitivity of the closed-loop system to perturbations can be successfully avoided by applying the proposed nonlinear control law.

In order to illustrate the performance of the nonlinear controller, Fig. 8 shows a series of numerical simulations using the control gains and initial conditions of the measurements in point A in Fig. 5. Since the control gains are selected from the linearly stable region, the small initial perturbation around the equilibrium lead to stable straight-line motion, regardless of the controller used. However, the larger initial perturbation causes the vehicle to spin out when the original, linear control law is used (panels (a)–(d)), similar to what was observed in the measurements. Parts of the simulated unstable trajectory where the lateral acceleration becomes exceedingly large are denoted by gray, indicating that these are beyond the capabilities of the vehicle model used. On the other hand, when the nonlinear control law is applied (panels (e)–(h)), the vehicle is able to safely steer itself towards the reference path, despite the large initial course angle. Here we used the saturation limit $\gamma_{\mathrm{sat}} = 15$ degrees. Notice that, since the wrapper function (18) affects the control actions for smaller desired steering angles too, the actual steering angle remained below 10 degrees during the whole simulation; see Fig. 8(g).

In order to show that despite the seemingly tight limitations on the steering angle, the nonlinear control law still allows the execution of highly dynamic vehicle maneuvers, one can calculate the lateral acceleration of the rear axle center point R as $a_{\mathrm{R}}^{\mathrm{lat}} = -\ddot{x}_{\mathrm{R}} \sin\psi + \ddot{y}_{\mathrm{R}} \cos\psi$. Using the equations of motion

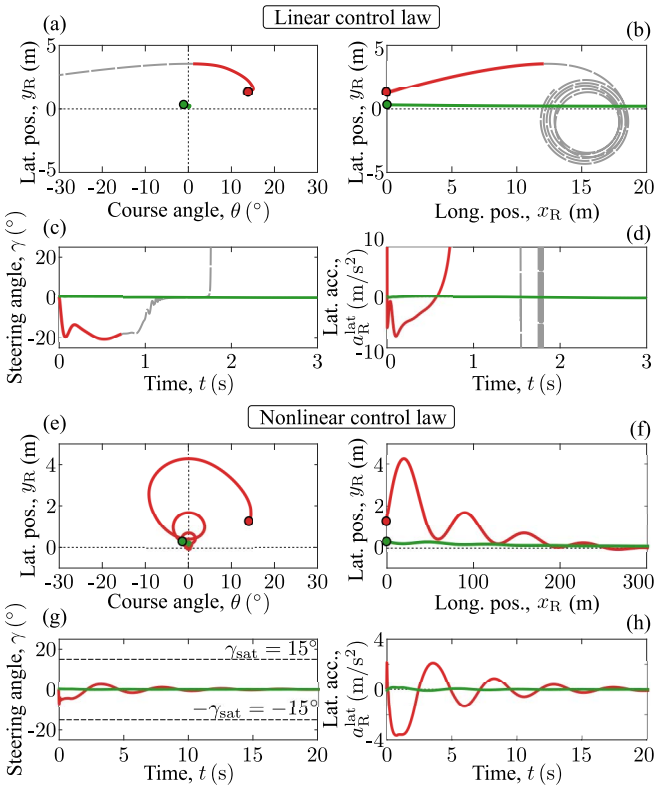

Fig. 8. Numerical simulations using the control gains and initial conditions of point A in Fig. 5.

of the vehicle model in Section II, the lateral acceleration reads

$$a_{\mathrm{R}}^{\mathrm{lat}} = \omega\left(\frac{V}{\cos\gamma} - (\sigma + l\omega)\tan\gamma\right) + \dot{\sigma}\,. \tag{19}$$

This is plotted in Fig. 8(d) when using the linear control law and in Fig. 8(h) when using the nonlinear control law. In the linear case the acceleration becomes exceedingly large, while in the nonlinear case its magnitude reaches around 4 m/s^2, which is executable by most production vehicles.

VI. Conclusion

Nonlinear analysis of the lane-keeping control of automated vehicles was performed in this letter. Using numerical collocation and continuation, unstable limit cycles have been identified and traced in the linearly stable domain of control gains. The oscillation amplitude of these periodic orbits around the equilibrium of stable path following was used as an indicator of the robustness of the controller against perturbations. Based on the results of the nonlinear analysis, a safe zone of control gains was identified, where the controlled vehicle was able to safely handle larger perturbations.

The results have been verified using a series of real-vehicle experiments on a test track. The measurement results confirmed the importance of taking into account the time delay as well as the nonlinear effects in the control design. Consistently stable measurements were only achieved in the region of the stable domain where the amplitude of the unstable limit cycle was sufficiently large. Outside of this region the system was demonstrated to be more susceptible to perturbations, which may lead to serious safety hazards in practice. To overcome these limitations, a nonlinear control law was proposed, which led to a significant increase of the amplitude of the unstable limit cycles and improved the robustness of the closed-loop system against perturbations. Therefore significantly better control performance was achieved when executing dynamic maneuvers.

The correspondence between the theoretical and experimental results could potentially be improved by using a higher fidelity vehicle model (e.g., a four-wheel model). In addition, the effects of external disturbances and road curvature will also be considered in future research.

References

[1] B. Olofsson and L. Nielsen, "Using crash databases to predict effectiveness of new autonomous vehicle maneuvers for lane-departure injury reduction," *IEEE Trans. Intell. Transp. Syst.*, vol. 22, no. 6, pp. 3479–3490, Jun. 2021.

[2] G. Heredia and A. Ollero, "Stability of autonomous vehicle path tracking with pure delays in the control loop," *Adv. Robot.*, vol. 21, nos. 1–2, pp. 23–50, 2007.

[3] I. Vörös and D. Takács, "Lane-keeping control of automated vehicles with feedback delay: Nonlinear analysis and laboratory experiments," *Eur. J. Mech. A*, vol. 93, May/Jun. 2022, Art. no. 104509.

[4] H. Lu, G. Stepan, J. Lu, and D. Takacs, "Dynamics of vehicle stability control subjected to feedback delay," *Eur. J. Mech. A*, vol. 96, Nov./Dec. 2022, Art. no. 104678.

[5] F. D. Rossa, G. Mastinu, and C. Piccardi, "Bifurcation analysis of an automobile model negotiating a curve," *Veh. Syst. Dyn.*, vol. 50, no. 10, pp. 1539–1562, 2012.

[6] S. Shen, J. Wang, P. Shi, and G. Premier, "Nonlinear dynamics and stability analysis of vehicle plane motions," *Veh. Syst. Dyn.*, vol. 45, no. 1, pp. 15–35, 2007.

[7] A. Steindl, J. Edelmann, and M. Plöchl, "Limit cycles at oversteer vehicle," *Nonlinear Dyn.*, vol. 99, no. 1, pp. 313–321, 2020.

[8] F. D. Rossa and G. Mastinu, "Analysis of the lateral dynamics of a vehicle and driver model running straight ahead," *Nonlinear Dyn.*, vol. 92, no. 1, pp. 97–106, 2018.

[9] G. Mastinu, D. Biggio, F. D. Rossa, and M. Fainello, "Straight running stability of automobiles: Experiments with a driving simulator," *Nonlinear Dyn.*, vol. 99, no. 4, pp. 2801–2818, 2020.

[10] Z. Liu, G. Payre, and P. Bourassa, "Stability and oscillations in a time-delayed vehicle system with driver control," *Nonlinear Dyn.*, vol. 35, no. 2, pp. 159–173, 2004.

[11] S. E. Li, H. Chen, R. Li, Z. Liu, Z. Wang, and Z. Xin, "Predictive lateral control to stabilise highly automated vehicles at tire-road friction limits," *Veh. Syst. Dyn.*, vol. 58, no. 5, pp. 768–786, 2020.

[12] J. Y. Goh, T. Goel, and J. C. Gerdes, "Toward automated vehicle control beyond the stability limits: Drifting along a general path," *J. Dyn. Syst. Meas. Control*, vol. 142, no. 2, 2020.

[13] J. Wurts, J. L. Stein, and T. Ersal, "Collision imminent steering at high speed using nonlinear model predictive control," *IEEE Trans. Veh. Technol.*, vol. 69, no. 8, pp. 8278–8289, Aug. 2020.

[14] S. Oh, S. S. Avedisov, and G. Orosz, "On the handling of automated vehicles: Modeling, bifurcation analysis, and experiments," *Eur. J. Mech. A*, vol. 90, Nov./Dec. 2021, Art. no. 104372.

[15] S. Beregi, S. S. Avedisov, C. R. He, D. Takacs, and G. Orosz, "Connectivity-based delay-tolerant control of automated vehicles: Theory and experiments," *IEEE Trans. Intell. Veh.*, early access, Dec. 1, 2021, doi: 10.1109/TIV.2021.3131957.

[16] W. B. Qin, Y. Zhang, D. Takács, G. Stépán, and G. Orosz, "Nonholonomic dynamics and control of road vehicles: Moving toward automation," *Nonlinear Dyn.*, vol. 110, pp. 1959–2004, Sep. 2022, doi: 10.1007/s11071-022-07761-4.

[17] T. Insperger and G. Stépán, *Semi-Discretization for Time-Delay Systems: Stability and Engineering Applications*. New York, NY, USA: Springer, 2011.

[18] Y. A. Kuznetsov, *Elements of Applied Bifurcation Theory*. New York, NY, USA: Springer, 1998.

[19] J. Sieber, K. Engelborghs, T. Luzyanina, G. Samaey, and D. Roose, "DDE-BIFTOOL manual—Bifurcation analysis of delay differential equations," 2014, *arXiv:1406.7144*.